

Searching for volcanic activity and a Mercury-like exosphere of the super-Earth HD3167 b

Eike W. Guenther,^{1*} Kristina G. Kislyakova²

¹ Thüringer Landessternwarte Tautenburg, Sternwarte 5, 07778 Tautenburg, Germany

² Department of Astrophysics, University of Vienna, Türkenschanzstrasse 17, 1180 Vienna, Austria

Accepted XXX. Received 2019 October 16; in original form 2019 August 29

ABSTRACT

HD3167 b is a transiting super-Earth that has a density which is consistent with a rocky composition. The planet is exposed to strong radiation, intense stellar wind, and likely strong tidal forces and induction heating. According to theory, planets that are so close to the star should have an atmosphere like Mercury but much more extended and denser. Other theories predict that such planets have a lava lake on their surfaces and exhibit an enormous volcanic activity. We have calculated the heating by electromagnetic induction to estimate if it can drive significant volcanic activity at HD3167 b and shown that for some magnetic fields the heating can be substantial. HD3167 is an ideal target to search for the exosphere of a planet, and signs of volcanic activity. We observed the planet in- and out-of transit with UVES in order to search for presence of lines originating from the exosphere of the planet such as the Na D_{1,2} and Ca II H&K lines as well as numerous [S II], [S III], and [O III] lines that are tracers of volcanic activity. We derived upper limits for the ratios of the line fluxes to the stellar flux. The upper limits that we derived are $I_{p,\lambda}/I_{*,\lambda} = 1.5 \cdot 10^{-3}$ for the Ca II H&K lines, and $I_{p,\lambda}/I_{*,\lambda} = 7.2 \cdot 10^{-4}$ and $I_{p,\lambda}/I_{*,\lambda} = 3.3 \cdot 10^{-4}$ for the Na D_{1,2} lines, respectively. The fact that our upper limits correspond to previous detections in 55 Cnc e shows that not all super-Earth show these lines all the time and that they might be variable.

Key words: stars: individual: HD3167 – planets and satellites: atmospheres – interiors – magnetic fields – terrestrial planets

1 INTRODUCTION

After the detection of giant exoplanets, the most exciting discovery was the detection of planets with masses of less than 15 M_{Earth} that have densities consistent with a rocky composition. A special class of such planets are transiting ultra-short-period planets which have orbital periods of one day or less. These planets have the advantage that due to their short periods, their masses and radii can be determined with high accuracy. Currently known transiting ultra-short-period planets (USPs) include CoRoT-7b (Léger et al. 2009), 55 Cnc e (Winn et al. 2011), Kepler-10b (Batalha et al. 2011), Kepler-78b (Sanchis-Ojeda et al. 2013), WASP-47e (Dai et al. 2015; Sinukoff et al. 2017a), KOI 1843.03 (Rappaport et al. 2013), K2-106 (Guenther et al. 2017), and HD3167b (discovery: Vanderburg (2016), characterization: Gandolfi et al. (2017)).

Although these planets are often called "super-Earths", the question is how Earth-like are they really? USPs are cer-

tainly exposed to very strong radiation and stellar wind. Because volatiles of their atmospheres are efficiently removed, such planets likely have only a thin atmosphere consisting of rocky vapors (Léger et al. 2011; Briot & Schneider 2010; Barnes et al. 2010). Léger et al. (2011) furthermore showed that the radiative as well as the tidal heating of these planets is so intense that it can drive extreme volcanism. Also, the temperature at the substellar point is so high that the surface rocks can melt and form a lava lake (Léger et al. 2009; Schäfer et al. 2009; Léger et al. 2011). The lava lake model can also explain the relatively high albedo of Kepler-10b (geometric albedo: 0.63 ± 0.09 , Bond albedo: $0.91^{+0.06}_{-0.10}$; Hu et al. 2015), because a lava composed of ThO₂ particles dispersed in the Al₂O₃ CaO would be almost as white as snow in the visible light (Rouan et al. 2011).

This type of lava is more plausible than the lava we have on Earth, because of its much higher melting point. Magma oceans are not only an exotic feature of USPs since most, if not all, rocky planets had magma ocean at a young age. Studying volcanic activity and lava oceans of USPs is thus not only important for these types of planets but also for

* E-mail: guenther@tls-tautenburg.de

understanding the evolution of rocky planets in general. For example, according to theory the outgassing from these lava oceans during their solidification produces CO₂- and H₂O-rich atmospheres (Elkins-Tanton, L.T. 2008, 2012; Lammer, et al. 2018). According to Ito et al. (2015) a planet with a rocky molten surface should have an atmosphere that is composed of gas-phase species dominated by Na, K, Fe, Si, SiO, O, and O₂.

USPs are not only heated by tides and the radiation of the star. Their interiors are also heated by electromagnetic induction if they are embedded in varying in time magnetic fields of their host stars (Kislyakova et al. 2018, 2017). In some cases, induction heating may even exceed the tidal heating. Since all stars with outer convective envelopes have magnetic fields, induction heating might be quite important for many of the short-period planets, which may then lead to enhanced volcanic activity. However, the amount of outgassing also depends on the mass of the planet. The highest level is expected for planets with masses between 2–3 M_⊕ (Dorn et al. 2018).

How can we possibly detect volcanic activity? Possible tracers for volcanism are the lines observed in Io and its plasma torus such as the [S III] 3722, [O II] 3726, [O II] 3729, [S II] 4069, [S II] 4076, [O III] 5007, [O I] 6300, [S III] 6312, [S II] 6716, [S II] 6731 Å lines, as well as the sodium D-lines (Brown & Chaffee 1945; Brown et al. 1975; Brown 1976; Brown & Shemansky 1982; Morgan & Pilcher 1982; Thomas 1993, 1996; Küppers & Jockers 1995, 1997; Kupo et al. 1976).

Some USPs are likely to have a Mercury-like exosphere, because light volatiles like H, He, O, CH₄ are quickly lost through the Jeans and other escape mechanisms. Since these planets are much larger and much closer to their host stars than Mercury, the amount of material released will be enormous. How can we detect the exosphere? Ca⁺ has been detected in the CaII H&K lines in the exosphere and coma of Mercury (Bida, Killen, Morgan 2010) and the Na coma has been detected during the Mercury transit in 2003 (Schleicher et al. 2004). Using this scaled-up model of Mercury and applying it to the close-in super-Earth CoRoT-7b, Mura et al. (2009) showed that CoRoT-7b should have a tail of escaping Ca⁺ particles. With a length of 30 R_{planet}, this tail is expected to have a column density larger than 10¹⁶ m⁻². Guenther et al. (2017) observed CoRoT-7b in- and out-of transit and obtained upper limits of the flux in Ca I, Ca II, and Na-lines that correspond to the most optimistic values in Mura et al. (2009). The main reason why neither volcanism nor the exosphere had been detected in CoRoT-7b is likely due to a large distance to its host star of 160.6 ± 0.9 pc, (Chiappetti et al. 2018).

Luckily, a number of USPs have been detected that orbit much closer stars. One of them is 55 Cnc which has a distance of 12.590 ± 0.012 pc (Chiappetti et al. 2018). The orbital period of the USP 55 Cnc e is 0.74 days. Its mass is 8.37 ± 0.38 M_{Earth}, and its radius 2.17 ± 0.10 R_{Earth}. The density of 5 Cnc e is 4.5 ± 0.20 g cm⁻³, which is roughly consistent with an Earth-like composition. Using optical transmission spectroscopy, Ridden-Harper et al. (2016) searched for an exosphere of this planet in the Na and singly ionized calcium Ca⁺ lines in the high resolution spectra obtained with HARPS. Combining the data of all five observed transits they detected a signal potentially associated with sodium in the planet’s exosphere at a statistical significance level of

3σ. Using the CaII H&K lines they also found a potential signal from ionized calcium at the 4.1σ-level. Interestingly, this latter signal originates from just one of the transit observations. This would correspond to an optically thick Ca⁺ exosphere with the size of approximately five Roche radii. If this were a real detection, it would imply that the exosphere exhibits extreme variability. Besides that, Demory et al. (2016) have used the middle IR wavelengths to search for volcanic activity on 55 Cnc e during secondary transits, with very promising results.

Other potentially interesting objects to search for the signatures of volcanism and an exosphere using optical transmission spectroscopy are K2-106 (Guenther et al. 2017) and HD3167 b (Vanderburg 2016; Gandolfi et al. 2017; Christiansen et al. 2017). What makes these objects interesting is that their densities are higher than that of 55 Cnc e. K2-106 b and HD3167 b have a density of 13.1^{-3.6}_{+5.4} and 8.00^{+1.10}_{-0.98} g cm⁻³, respectively. The density of HD3167 b is consistent with a composition containing up to 40% iron and 60% silicate, and K2-106 b to the composition containing possibly up to 70% iron (Gandolfi et al. 2017; Guenther et al. 2017). For comparison, the Earth has an iron contents of 32.5% and Mercury of 70%. HD3167 b is the preferred target, because its host star is 13 times brighter than CoRoT-7. HD3167 b has an orbital period of 0.96 days, a semi-major axis of 0.01752 ± 0.00063 AU, a mass of 5.69 ± 0.44 M_{Earth}, a radius of 1.574 ± 0.054 R_{Earth}, and an equivalent temperature of T_{eq} = 1759 ± 20 K. The outer component, HD3167 c, has an orbital period of 29.8 days, a mass of 8.33^{+1.79}_{-1.85} M_{Earth} and a radius of 2.74^{+0.11}_{-1.00} R_{Earth} (Gandolfi et al. 2017). The orbit of HD3167 c is highly inclined with respect to the stellar rotation axis (Dalal et al. 2019). Because the orbital inclinations of the two planets are rather similar with i = 88.6^{+1.0}_{-1.4} deg, and i = 89.6 ± 0.2 deg, and since most systems are co-planar (Winn et al. 2015), we assume that also HD3167 b has a highly inclined orbit. As we will discuss in this article, the highly inclined orbit makes this planet particularly interesting for studies on the planet-star interactions and induction heating.

According to Christiansen et al. (2017), possibly a third non-transiting planet, HD3167 d, exists between the two transiting ones. The planet is supposed to have an orbital period of 8.51 days and a K-amplitude of 2.39 ± 0.24 ms⁻¹, which corresponds to a minimum mass of 6.90 ± 0.71 R_{Earth}. However, the radial-velocity (RV) signal of this planet was not detected by Gandolfi et al. (2017). Instead they found two adjacent signals with periods of 6.0 and 10.8 days and K-amplitudes of 1.34^{+0.27}_{-0.28} and 5.967^{+0.038}_{-0.035} ms⁻¹. Whether there is a planet with a different inclination between the two transiting ones is thus uncertain. The host is a K0V-star with a rotation period of 23.52 ± 2.87 d that has a distance of only 47.4 ± 0.2 pc (Chiappetti et al. 2018).

In this article we present the analysis of in-transit and out-of-transit spectra of HD3167 b obtained in order to search for the exosphere and the volcanic activity of this planet. We discuss observations in Section 2, the data reduction in Section 3, and the results in Section 4. We discuss possible origins of the atmosphere and calculate possible induction heating rates in Section 5. Sections 6 contains the discussion and Section 7 our conclusions.

2 OBSERVATIONS

We observed HD3167 continuously on November 20, 2017 from UTC 00:34 until UTC 04:33 with UVES (Ultraviolet and Visual Échelle Spectrograph) at the VLT (ESO program 099.C-0175(A)). This corresponds to Heliocentric Julian Dates (HJD) from 2458077.52361 to 2458077.68958. The transit occurred from HJD 2458077.595261 to 2458077.664011 (Vanderburg 2016). UVES is the Échelle spectrograph for the UT2 KUEYEN Telescope at the ESO Paranal (Dekker et al. 2000) and has two arms. The wavelength ranges of the two arms are 3259 to 4493 Å (the "blue" arm) and 4726 to 6835 Å (the "red" arm). The resolution of the spectra is $\lambda/\Delta\lambda = 52000$, or 5.5 km s^{-1} , and the dispersion typically $1.0 \text{ km s}^{-1} \text{ pixels}^{-1}$. During the four hours of observations 58 spectra were obtained in the blue channel and 65 in the red channel. The exposure times in the blue and red channel were 200 s, and 200 s (first 13 frames) and 150 s (all other frames), respectively.

3 REDUCTION OF THE DATA

The standard EsoReflex pipeline was used for the basic data reduction which includes the bias subtraction, the flat-fielding, the extraction of the spectra and the wavelength-calibration (Møller Larsen et al. 2019). Additionally to these, we also reduced the spectra using IRAF (Image Reduction and Analysis Facility) to find out whether that makes any difference. Both types of reduced spectra were essentially identical. After these initial steps have been done, we carried out seven additional steps to extract the signal of the planet. We describe this procedure below.

i.) UVES is a slit spectrograph. The Thorium-Argon hollow cathode lamp used for the initial wavelength calibration is placed right in front of the spectrograph and not at infinity. The initial wavelength-calibration, which is based on the Thorium-Argon lamps, thus has a small shift with respect to the true wavelength. The first step thus was to determine this instrumental shift using the telluric lines, and to correct each spectrum for it.

ii.) The next step was to model the telluric lines. This was done using the ESO molecfit tool (Noll et al. 2019). The strength of the telluric lines varies with the airmass and the weather conditions. For example, the H_2O lines become stronger if the humidity, or the airmass increases during the observations. The airmass was 1.169 at the beginning of the observations and 1.754 at the end. The precipitable water vapor (PWV) was 2.0 mm until HJD 2458077.60, and then decreased down to 1.3 mm at HJD 2458077.64. After that the level increased again and reached 1.6 mm at the end of the observations. On average the PWV was only 1.76 ± 0.28 mm. Fig. 1 shows as example the normalized spectrum of HD3167 (black line) together with telluric spectrum calculated with molecfit for PWV of 2.0 mm. The model also contains all other lines of the Earth atmosphere. Due to the dry conditions the H_2O lines were weak and it was thus easy to remove them.

iii.) The next step was to flux-calibrate the spectra using the known spectral energy distribution of the star. We calculated the flux of the star at the distance of the Earth in W m^{-2}

per wavelength interval, as well as the total flux emitted by the star in Watt per wavelength interval.

iv.) Given that we expected that any lines from the planet were a hundred, or perhaps a thousand times weaker than the stellar lines, the subtraction of the stellar spectrum was an important step. We tried out several different methods. We subtracted and also divided the observed spectrum by the average spectrum. In the following sections, we present the results after subtracting the averaged stellar spectrum not the ratio of the two spectra. The reason is that the resulting spectrum then has the unit W m^{-2} (per wavelength interval). If we would use the ratio, the spectrum would be dimensionless. However, before we can subtract the average stellar spectrum, we have to find out if it varies during the observations. A stellar spectrum can change if the activity-level of star changes. This is for instance the case if a stellar spot rotates into view, or if new spots appear on the stellar surface. Since HD3167 has a rotation period of 23.52 ± 2.87 days, it rotated only by 2.5 degrees during the observations. It is thus unlikely that a new spot rotated into view. The lifetimes of spots for stars with similar rotation periods are about 100 days (Namekata et al. 2019). It is thus also unlikely that an active region appeared on the visible surface during the four hours of observations. Using the Mt. Wilson S_{HK} -index, we can also determine the variations in the activity level during the observations. In this way we find out whether plage regions, which are usually associated with spots, appeared on the stellar surface during the observations. A third reason why a stellar spectrum can change are flares. Flares also show up in the CaII H&K lines. Thus, S_{HK} -index shows us whether plagues, or spots appeared or disappeared on the stellar surface, and whether there were any flares. HD3167 is a very inactive star. Vanderburg (2016) determined a Mt. Wilson S_{HK} -index of 0.178 ± 0.005 and the Mt. Wilson log R_{HK} -index of -4.97 ± 0.02 . We found a S_{HK} -index of 0.1779 ± 0.0011 out-of transit and 0.1782 ± 0.0007 ¹ during transit. The activity level thus did not change significantly during the observations and, therefore, it is justified to average the out-of transit spectra of the star. Fig. 2 shows an individual spectrum before and after the subtraction of the average spectrum of the host star. This spectrum was obtained at UT 03:07, or roughly at the middle of the transit. The figure shows the region containing the [SII] lines at 6716.440, and 6730.816 Å (positions marked). We also show the spectrum rebinned to the resolution of the spectrograph.

v.) Before we can add up the spectra taken in- and out-of transit, we have to shift them according to the RV of the planet. Using the values published by Gandolfi et al. (2017), we calculate that the RV of the planet changes during transit from -43.7 ± 3.3 to $+43.7 \pm 3.3 \text{ km s}^{-1}$ with respect to the star. If we use the values from Christiansen et al. (2017), it is -44.5 ± 3.4 to $+44.5 \pm 3.4 \text{ km s}^{-1}$. The difference between the two is thus smaller than the errors given in the publications. On average, the RV of the planet changes by 3.3 km s^{-1} from spectrum to spectrum with respect to the star².

¹ Relative error of the measurement, not the absolute value of the index.

² When planing the observation, we calculated how long the exposure time could be, before the spectral-lines of the planet would be smeared out by one the resolution element of the spectrograph.

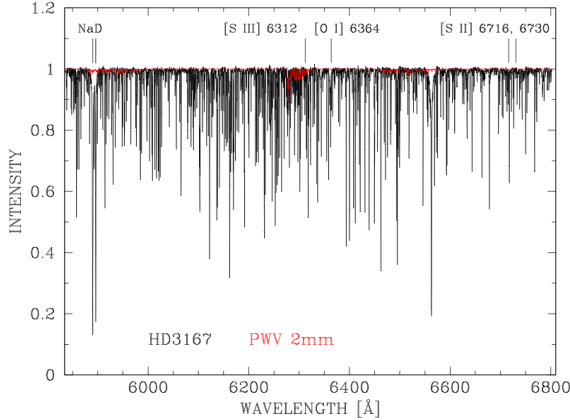


Figure 1. Normalized spectrum of HD3167 in the red channel (red line) together with the telluric spectrum (black line) as calculated by molecfit for precipitable water vapour (PWV) of 2.0 mm.

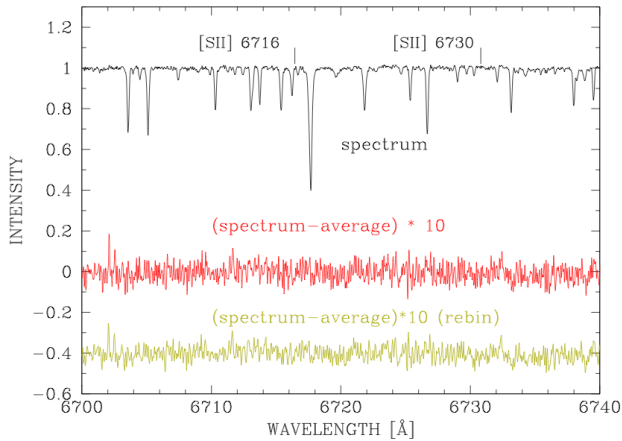


Figure 2. Step of the reduction of the frame taken at 03:07:22. The black line is the observed spectrum before subtracting the average stellar spectrum. The red line is the magnified spectrum after the subtraction. The yellow line is the same but rebinned to the resolution of the spectrograph.

vi.) After computing the weighted average of the spectra taken in- and out-of transit, we cut out the regions that we were interested in. These are the regions centered on the diagnostic lines mentioned in Section 1, and listed in Table 1.

vii.) The final step was to measure the flux of the lines using IRAF-tool *sbands*. We used an extraction width of 10.3 km s^{-1} for the lines. The reason for this width is that we have to take the combined effects of finite resolution of the spectrograph (5.5 km s^{-1}), the shift of the planet during the exposure (3.3 km s^{-1}), and the error of the RV-amplitude (typically less than 3.4 km s^{-1}), plus the errors of these values into account. The length of the continuum strips is always 100 km s^{-1} . After integrating along wavelength, we obtain the fluxes of the lines in W m^{-2} , and W , respectively. The results are given in Table 1.

4 RESULTS

The results are presented in Figs. 3 to 11. Each figure presents a spectrum for one of the spectral lines listed in Table 1. The red lines in these figures are the residuals of the in-transit spectra after subtracting the stellar and telluric spectra. In other words, the red-lines are the spectra of the planet.

The blue lines are the residuals of the out-of transit spectra. They should not contain any spectral lines of planetary origin. We show these spectra as a reference for the noise level of the residual spectra.

We use the units of km s^{-1} for the wavelength rather than Å , because the resolution of an Échelle spectrograph is almost constant in velocity over the whole observed wavelength range (5.5 km s^{-1}), and also because it makes it easy to see where the line from the planet should be. The line originating from the planet would be centered at zero velocity and would have a width of 10.3 km s^{-1} , given the resolution of the spectrograph, the RV-shift of the planet during the exposure and taking the error of the RV-amplitude into account.

Since the spectra are flux-calibrated, in principle the unit on the Y-axis is Watt per wavelength-interval. However, since we like to show the residual spectra together with the spectrum of the star, we have to magnify the residual spectra by a factor of 100 (a factor of 50 for the CaII H,K lines). Thus, one unit of the residual spectra corresponds to 10^{-2} (2×10^{-2} for the CaII H,K lines) of the continuum flux of the star. In order to show the different spectra more clearly, we moved the red and the blue lines upwards so that the spectra are well separated. The scale of the residual spectra is shown at the upper left corner in each figure.

We also show the stellar spectrum (black line) in Figs. 3 to Fig. 11 to demonstrate the location of the stellar lines. The noise level is higher at those wavelengths where the star has deep lines. However, since the spectrum of the star moved from -44.5 ± 3.4 to $+44.5 \pm 3.4 \text{ km s}^{-1}$ with respect to the spectrum of the planet, the effect from the deep stellar lines was significantly reduced.

We measured the flux in a region with a width of 10.3 km s^{-1} at the position of each spectral line. The upper limits for the fluxes of the lines emission are given in Table 1, and the system's parameters in Table 2. The first two columns give the identification of the line and the wavelength. The third column shows the line fluxes from the planet relative to the flux of the star at that line ($I_{p,\lambda}/I_{*,\lambda}$). The significance of the result is given in the fourth column. Since all values are below 3σ , none of the lines were detected and we consider the values in the fourth column as upper limits. The upper limits that we derive are approximately 1.5×10^{-3} for the CaII H,K lines and 7.2×10^{-4} and 3.3×10^{-4} for the NaD_{1,2} lines, respectively. For comparison, [Ridden-Harper et al. \(2016\)](#) detected the CaII H,K in 55 Cnc e at a level of $I_{p,\lambda}/I_{*,\lambda} = 7 \times 10^{-2}$ and $I_{p,\lambda}/I_{*,\lambda} = 2.3 \times 10^{-3}$ the NaD_{1,2} lines, respectively. Thus, our upper limits are even lower than the $I_{p,\lambda}/I_{*,\lambda}$ -values for 55 Cnc e.

5 POSSIBLE ORIGIN OF THE ATMOSPHERE

There are several mechanisms to produce an atmosphere on a close-in rocky exoplanet. First, the atmosphere can

Table 1. Upper limits of the line fluxes from the planet

line	λ [Å]	$I_{p,\lambda}/I_{*,\lambda}$	significance ¹ σ	observed [Wm^{-2}] 3σ upper limits	total emission [W] 3σ upper limits	remarks ²
CaII K	3933.666	-0.00153 ± 0.00085	1.8	$< 4.5 \times 10^{-20}$	$< 1.2 \times 10^{18}$	55 Cnc e
CaII H	3968.468	-0.00156 ± 0.00097	1.6	$< 5.6 \times 10^{-20}$	$< 1.5 \times 10^{18}$	55 Cnc e
[SII]	4068.600	-0.0039 ± 0.0020	2.0	$< 7.3 \times 10^{-19}$	$< 1.9 \times 10^{19}$	Io
[SII]	4076.349	-0.0003 ± 0.0020	0.2	$< 7.5 \times 10^{-19}$	$< 2.0 \times 10^{19}$	Io
CaI	4226.728	-0.024 ± 0.024	1.0	$< 3.4 \times 10^{-18}$	$< 9.2 \times 10^{19}$	Io, Mercury
[OIII]	4356.794	-0.0036 ± 0.0020	1.8	$< 9.2 \times 10^{-19}$	$< 2.5 \times 10^{19}$	
[OIII]	5006.843	-0.0001 ± 0.00045	0.2	$< 2.4 \times 10^{-19}$	$< 6.4 \times 10^{18}$	Io
NaD ₂	5889.953	0.00033 ± 0.00040	0.8	$< 2.4 \times 10^{-19}$	$< 6.5 \times 10^{18}$	Io, 55 Cnc e, Mercury
NaD ₁	5895.923	0.00072 ± 0.00027	2.6	$< 1.7 \times 10^{-19}$	$< 4.5 \times 10^{18}$	Io, 55 Cnc e, Mercury
[SIII]	6312.06	-0.00003 ± 0.00046	0.1	$< 2.7 \times 10^{-19}$	$< 7.3 \times 10^{18}$	Io
[OI]	6363.776	0.00033 ± 0.00029	1.1	$< 1.7 \times 10^{-19}$	$< 4.6 \times 10^{18}$	
[SII]	6716.440	0.00040 ± 0.00029	1.4	$< 1.8 \times 10^{-19}$	$< 4.8 \times 10^{18}$	Io
[SII]	6730.816	0.00040 ± 0.00032	1.2	$< 2.0 \times 10^{-19}$	$< 5.4 \times 10^{18}$	Io

¹ All excesses below 3σ are considered insignificant and taken as upper limits.

² Examples for objects where this line has been detected.

$I_{p,\lambda}/I_{*,\lambda}$ is the intensity of the planet in respect to the star at the wavelength of the spectral-line.

Table 2. Parameters of the star HD 3167 and planet HD 3167b taken from (Gandolfi et al. 2017).

Parameter	Value
Stellar mass [M_{\odot}]	0.877 ± 0.024
Stellar radius [R_{\odot}]	0.835 ± 0.026
Stellar age [Gyr]	5.0 ± 4.0
Stellar equilibrium temperature [K]	5286 ± 40
Stellar rotational period [days]	23.52 ± 2.87
Distance to the system [pc]	45.8 ± 2.2
Planetary mass [M_{\oplus}]	5.69 ± 0.44
Planetary radius [R_{\oplus}]	1.574 ± 0.054
Planetary equilibrium temperature [K]	1759 ± 20
Semi-major axis [au]	0.01752 ± 0.00063
Inclination [degree]	$88.6^{+1.0}_{-1.5}$

be generated by volcanic activity driven by internal heating sources, and second, if the temperature on the surface is high enough, the rocks on the surface can melt thus creating a mineral atmosphere. In this section, we discuss both mechanisms of atmosphere formation.

Volcanic activity of a planet requires an internal heating source as a driver. There are several sources of internal energy known for planets: heat is produced due to radioactive decay, mantle differentiation, core and inner core formation, tidal heating, and induction heating. The first four of these mechanisms are the dominant ones in the Earth. They can be very important for young planets, but the old age of HD3167b indicates that these heating sources are likely not the dominant ones at present (Noack et al. 2016). The latter two mechanisms, while insignificant for the Earth, can be very powerful in planets orbiting close to their host stars. From the observations of Io we know that a powerful internal heat source can drive enormous volcanic activity (Peale 1979). Tidal heating, to be substantial, requires an eccentric or inclined orbit of a planet. Since the orbit of HD3167b is likely highly inclined, one can expect this heating source to be quite important for HD3167b (Beuthe 2013). However, due to a relatively high mass of HD3167b, volcanic outgassing from this planet is likely inefficient (Noack et al.

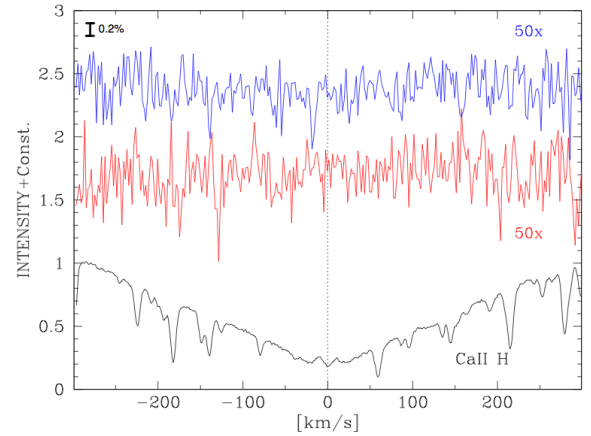


Figure 3. Average residual spectrum in the CaII H line after subtracting the average out-of-transit spectrum of the star. As explained in the text, the red line is the residual of the in-transit spectrum, in other words, the spectrum of the planet. The blue line is the residual of the out-of-transit spectrum. We magnified the residuals by a factor of 50 so that the signal can be seen. The scale for the red and blue lines is shown at upper left corner. The black line is the stellar spectrum.

2017; Dorn et al. 2018). Dorn et al. (2018) have shown that at small masses (below 2-3 M_{\oplus}) outgassing positively correlates with the planet's mass, since it is controlled by volume of the mantle, but at higher masses outgassing decreases with the planet's mass, which is due to the increasing pressure gradient that limits melting to shallower depths. Since tidal heating produces heat mostly deep in the planetary mantle, it can not melt the mantle of a planet as massive as HD3167b. Therefore, we can conclude that even though one can expect strong tidal heating in the interiors of HD3167b, it can unlikely drive strong volcanic activity on this planet.

Another newly identified heating source for exoplanets is induction heating (Kislyakova et al. 2017). Electromagnetic induction is the production of voltage across an electrical conductor if the magnetic field around it varies in time.

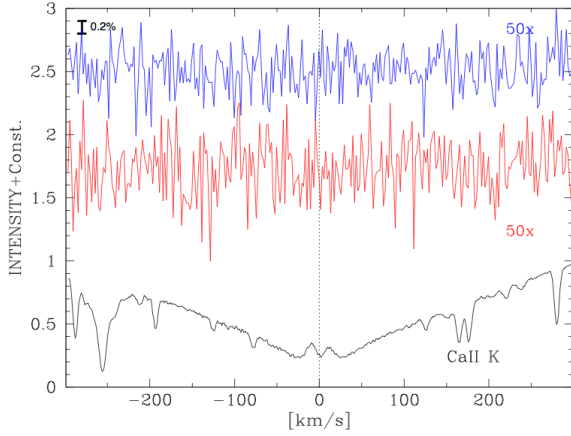


Figure 4. Same as Fig. 3 but for CaII K line.

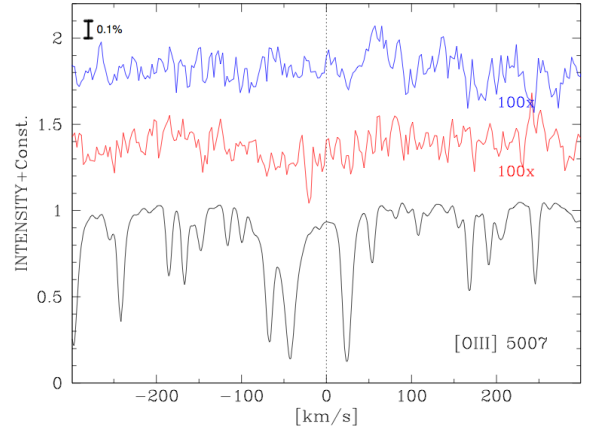


Figure 7. Same as Fig. 5 but for [OIII] 5007 line.

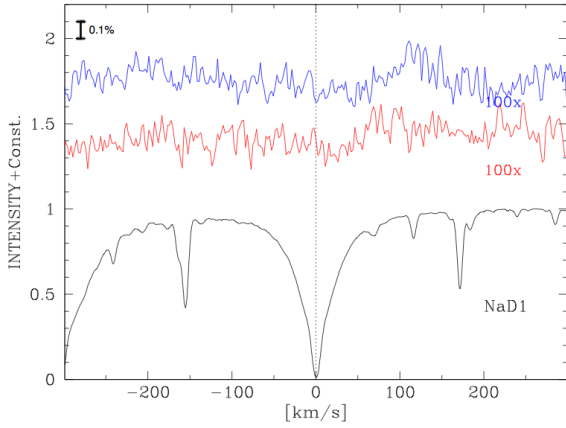


Figure 5. Same as Fig. 3 but for NaD₁ line and the residuals magnified by a factor of 100. One unit thus corresponds to 10^{-2} of the continuum level of the star.

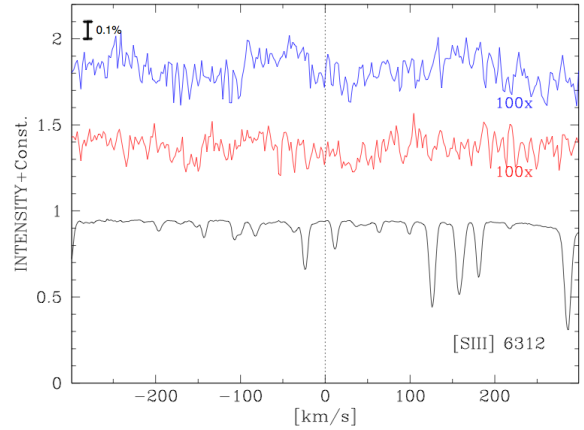


Figure 8. Same as Fig. 5 but for the [SIII] 6312 line.

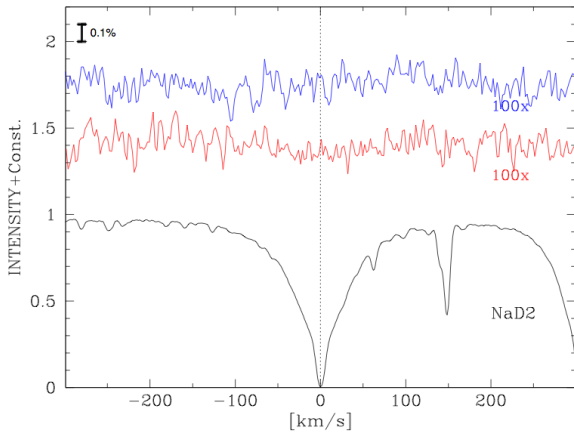


Figure 6. Same as Fig. 5 but for NaD₂ line.

This voltage, or electromotive force, generates alternating currents flowing inside the body, which then dissipate and produce heat inside the conductor. This heating source requires a presence of a strong varying magnetic field around the planet. For HD3167 b, the source of the variation of the magnetic field around the planet is the planetary motion on its highly inclined polar orbit. [Kislyakova et al. \(2018\)](#) have shown that induction heating can be very substantial for planets on inclined orbits, if the stellar magnetic field is strong enough. Below we calculate the power of induction heating inside HD3167 b. We have followed the procedure described in [Kislyakova et al. \(2018\)](#) for a planet on an inclined orbit.

First, we have calculated the density and electrical conductivity profiles for HD3167 b using the code CHIC ([Noack et al. 2016](#)) that are shown in Fig. 12. We have assumed a composition with a slightly higher iron content than that of the Earth, namely, of 40%. We further assumed that the iron accumulates in the planet's core. Electrical conductivity has been calculated for a given composition of a mineral layer in the mantle and for a calculated temperature profile. We have assumed the equilibrium temperature of HD3167 b at its surface as a boundary condition (see Table 2). We have used the procedure to calculate induction heating in a

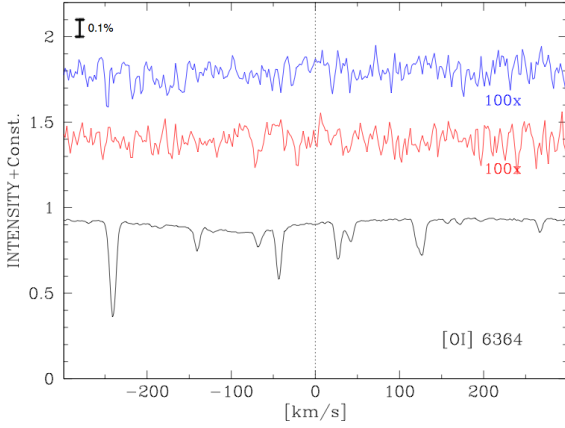


Figure 9. Same as Fig. 5 but for the [OI] 6364 line.

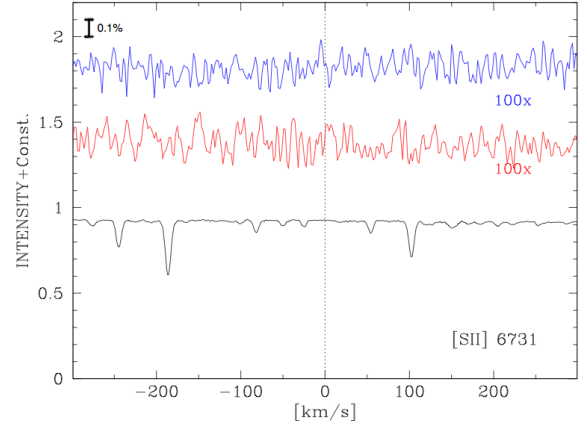


Figure 11. Same as Fig. 5 but for the [SII] 6731 line.

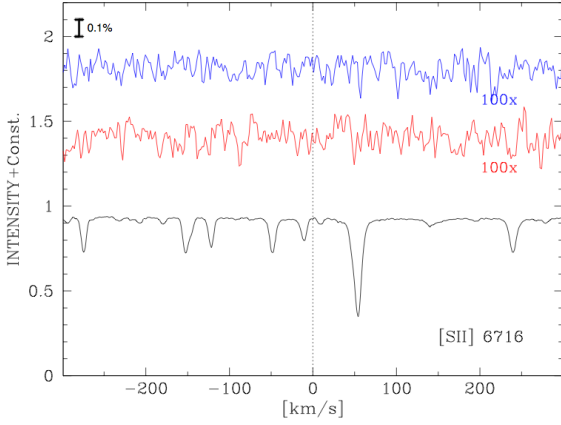


Figure 10. Same as Fig. 5 but for [SII] 6716 line.

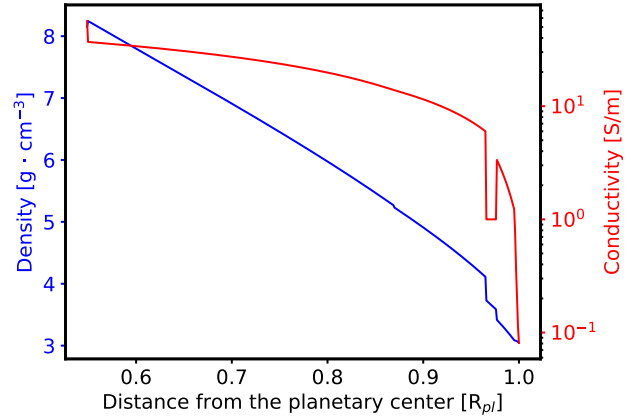


Figure 12. Density (blue) and electrical conductivity (red) profiles for HD3167b calculated with the interior model CHIC (Noack et al. 2016).

planet with a conductivity varying with depth, as described in Kislyakova et al. (2017). In this model, induction equation is solved in every layer, and the conductivity values at the surface and in the planetary core are used as boundary conditions. We also need the strength of the stellar magnetic field as an input parameter. Although the magnetic field of HD3167 has not been measured, one can conclude from its old age of 5 Gyr and a relatively slow rotational period of 23 days that this star likely has a relatively low magnetic field. Following Vidotto et al. (2014) and the observations of the Sun, which is also an inactive star, we have assumed the strength of the global dipole component of the stellar magnetic field of 2-5 G. Although higher harmonics of the stellar magnetic field can also be present, we have not considered them here. They are unlikely to produce a strong heating effect due to their sharp decline with the distance to the star.

The results of our calculation are presented in Fig. 13. The figure shows internal heating rates inside HD3167b for three values of the stellar dipole field: 1, 5, and 50 G. These cases correspond to the total energy release inside HD3167b of 1.8×10^{19} , 4.5×10^{20} , and 4.5×10^{22} erg s^{-1} , respectively. While the first two values are typical for an old, inactive star, the last value has been selected to illustrate possible

induction heating in the planet when this stellar system was young. The dashed line indicates an approximate limit of the internal heating rate necessary to melt the planetary mantle, if the planet is exposed to this amount of heating for a geologically long time (Kislyakova et al. 2017). Note that this limit can vary within approximately 10^{-6} – 10^{-8} erg g^{-1} s^{-1} , with the lower value more typical for small planets. Unlike tidal heating which leads to energy release deep in the planetary mantle, induction heating (or skin effect) preferentially heats the very upper part of the planetary mantle. According to Dorn et al. (2018), this indicates that in this case some melt and, therefore, some volcanic activity could be produced, because the pressure in the upper mantle is not yet so high that it would suppress the melt formation. Our non-detection of traces of volcanic activity indicates that the global magnetic field of HD 3167 is likely weak and of the order of only 1-2 G. We can also conclude that induction heating must have been stronger in HD3167b in the past when the stellar magnetic field was stronger. At present, the exosphere of HD3167b is likely generated by the melting of the surface rocks by intense stellar radiation.

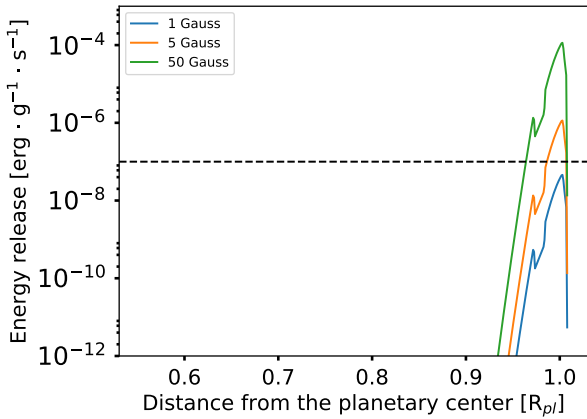


Figure 13. Induction heating inside HD3167 b for three values of the stellar magnetic field: 1, 5, and 50 G. The present-day global magnetic field of HD 3167 is likely weak and close to 1 G. The picture shows the heating rates inside the planet. The dashed line indicates an approximate limit necessary to melt the rocks on a geological time scale.

6 DISCUSSION

The architecture of the HD3167-system is unusual, which makes the system an interesting target for many different studies. HD 3167 b is a transiting planet with an orbital period of 0.96 days, and an inclination of $i = 88.6^{+1.0}_{-1.5}$ degrees. The next outer planet is supposed to be the non-transiting planet HD 3167 d. However, as we pointed out above, it is not certain that this planet exists. The third, or perhaps second planet of the system is the transiting planet HD3167 c which has an orbital period of 29.8 days and $i = 89.6 \pm 0.2$ degrees. Recently, Dalal et al. (2019) found that HD3167 c is in a nearly polar orbit. Since most planetary systems are coplanar, HD3167 b should also have a nearly polar orbit.

Because induction heating requires the magnetic field at the position of the planet to vary, a system with planets in polar orbits is a good target for studying induction heating (Kislyakova et al. 2018, 2017). HD3167 is also a good target, because it is a nearby, bright star that allows to take high precision measurements.

However, induction heating also depends on the strength of the magnetic field of the star. The rotation period of HD3167 is 23.52 ± 2.87 days and the activity index $\log R'_{\text{HK}} = -5.04$. For comparison, the Sun has $\log R'_{\text{HK}} = -4.96$ and a rotation period of 25 days (Wright et al. 2004). There are 21 photometric measurements of HD3167 in the APPLAUSE¹ data-base. The average brightness of the star is $V = 9.03 \pm 0.10$ mag. Given that the average error of the photometry is 0.15 mag, the stars is, within errors, not variable. This is also consistent with a star of a solar activity level. The activity level of HD 3167 is basically the same as the Sun. We thus concluded (Section 5) that at present neither induction nor tidal heating are capable to produce significant volcanic outgassing on HD3167 b. This is in agreement with a non-detection of sulfur lines in our observations, since sulfur is mostly produced by classical volcanic outgassing.

¹ <https://www.plate-archive.org/applause>

This leaves the third possibility for the atmosphere production, namely, a mineral atmosphere, which is produced due to melting of the surface crust by intense stellar radiation (Schäfer et al. 2009). The high equilibrium temperature of HD3167 b of $T_{\text{eq}} = 1759 \pm 20$ K suggests that it should indeed have a tenuous mineral atmosphere (Ito et al. 2015; Miguel et al. 2011), likely dominated by sodium and oxygen (Miguel et al. 2011).

How meaningful are the upper limits derived? Apart from the Earth and Venus, where traces of ongoing volcanic activity have recently been identified (Shalygin 2015), Io is the only other object in the solar system that has active volcanism. Sulfur ejected from Io forms a plasma ring around Jupiter, known as the Io plasma torus. Our non-detection of volcanic activity on HD3167 b indicates that the magnetic field of HD 3167 is likely weak, which is consistent with the relatively slow rotation and the low X-ray brightness of the star.

On Io, Morgan & Pilcher (1982) have detected fluxes of 215 ± 28 Rayleigh for the [SII] 6731 Å which corresponds to a total emission of 5×10^{15} W. Our upper limit for that line is 5.4×10^{18} W and thus a factor of 1000 higher. However, we should keep in mind that HD3167 b has 5.5 times the radius and 30 times the surface area of Io, and that the internal and external heating of HD3167 b is supposed to be correspondingly stronger. It is thus reasonable to assume that the lines could also be much stronger. The non-detection of a volcanic atmosphere caused by tidal heating agrees with the results by Noack et al. (2017) and Dorn et al. (2018) that massive planets do not exhibit efficient outgassing. Demory et al. (2016) have also argued that the height of volcanic plumes can not be much higher than about 10 scale heights in the atmosphere, corresponding to a few hundred km in the case of the a super Earth. If this is true, it would be very difficult to detect a volcanic atmosphere in any super Earth.

We can also follow Ridden-Harper et al. (2016) and calculate the size of the absorption region and compare it to the size of the Hill-sphere for an optically thick line. For the Ca⁺ exosphere in 55 Cnc e they found that it is approximately five times larger than the Roche lobe radius, or about $8 R_{\text{Hill}}$. For NaD they found roughly a Roche lobe radius, or $1.5 R_{\text{Hill}}$. The 3σ upper limits correspond to a regions of 0.4-0.5 Hill spheres for the CaII H,K lines and 0.1-0.3 Hills spheres the NaD lines. Our upper limits are thus smaller than size of these regions in 55 Cnc e.

We can also compare our upper limits of the line-fluxes with the total amount of radiation that the planet receives, because radiative heating from the star should be one of the main energy sources of the volcanism. The upper limits for the lines are typically 500-1000 times smaller than the radiation that the planet receives from the star which is 2.9×10^{21} W.

In our observations, we have searched for both sodium and oxygen lines, but we were only able to obtain upper limits for the signal. We argue that because of the relatively high mass, and the relatively low magnetic field strength, detecting the signature of volcanism is very difficult. This is consistent with our measurements. An ideal target would be a lower mass USP orbiting an active star with a stronger magnetic field, or a lower mass USP on an eccentric or inclined orbit. As we have shown, an object like HD3126 but with a magnetic field strength of 50 Gauss would be perfect.

The prospects for detecting volcanism are better for planets of M-stars because these tend to have higher magnetic field strength than solar-like stars.

The best objects to detect mineral atmospheres are planets with high equilibrium temperatures, likely higher than that of HD3126 b. However, HD3167 b still is an interesting target for detection of a mineral atmosphere. We note that in the case of 55 Cnc e, the CaII H&K line were detected in only one of the five transit observed. If the signal is that variable as in 55 Cnc e it might well be that these lines are also detected in HD3167 b if the observations are just repeated several times.

7 CONCLUSIONS

HD3167 b is one of the best targets to search for volcanic activity and a Mercury-like exosphere of a rocky planet. It is not only a planet that orbits at a very short distance from the star, also its host star is only at a distance of 47.35 ± 0.15 pc (Chiappetti et al. 2018). Recent observations have furthermore shown that HD3167 c is in a polar orbit which makes it very likely that also HD3167 b is in a polar orbit. Thus, this planet is not only radiatively and tidally heated but also induction heating is possible. We have obtained high-resolution spectra of HD3167 b in- and out-of-transit and searched for emission or absorption lines tracing volcanic activity and a Mercury-like exosphere. Although we derived only upper limits, these are basically similar to fluxes of the NaD and CaII H&K lines in 55 Cnc e obtained by Ridden-Harper et al. (2016). An interesting aspect of the detection of the CaII H&K line in 55 Cnc e is that it was only detected in one of the five transits observed. It could thus well be that the same lines could also be detected in HD3167 b if more observations are conducted. We conclude that the most likely atmosphere of HD3167 b is a mineral atmosphere produced by the melting of the rocky surface by intense stellar radiation. Induction heating can lead to some outgassing if the stellar magnetic field is strong enough. However, volcanic outgassing is likely to be quite small because of the relatively large mass of this planet which leaves the mineral atmosphere produced by the melting of the surface rocks by intense stellar radiation as the most probable mechanism of the atmosphere formation at HD3167 b. Hopefully future observations can help us to find out what kind of atmosphere of HD3167 b has.

ACKNOWLEDGEMENTS

We are very thankful to the ESO-staff for carrying out the observations in service mode, and for providing the community with all the necessary tools for reducing and analyzing the data. This work was generously supported by the Thüringer Ministerium für Wirtschaft, Wissenschaft und Digitale Gesellschaft. This research has made use of the SIMBAD database, operated at CDS, Strasbourg, France. This work has made use of data from the European Space Agency (ESA) mission *Gaia* (<https://www.cosmos.esa.int/gaia>), processed by the *Gaia* Data Processing and Analysis Consortium (DPAC, <https://www.cosmos.esa.int/web/gaia/dpac/consortium>). Funding for

the DPAC has been provided by national institutions, in particular the institutions participating in the *Gaia* Multilateral Agreement. KK acknowledges the support from the Austria Science Fund (FWF) NFN project S116-N16 and the subproject S11607-N16. The authors are grateful to Prof. Lena Noack for providing the electrical conductivity profile of HD 3167b. We also acknowledge the use of the APPLAUSE data-base. Funding for APPLAUSE has been provided by DFG (German Research Foundation, Grant), Leibniz Institute for Astrophysics Potsdam (AIP), Dr.-Reimei Sternwarte Bamberg (University Nürnberg/Erlangen), the Hamburger Sternwarte (University of Hamburg) and Tartu Observatory. Plate material also has been made available from Thüringer Landessternwarte Tautenburg.

REFERENCES

- Barnes et al. 2010, ApJ 709, 95
 Batalha, N.M., Borucki, W.J., Bryson, S.T., et al. 2011, ApJ, 729, 27
 Beuthe, M. 2013, Icarus, 223, 308
 Bida, Killen & Morgan, Nature 404, 159, 2000
 Briot, D., & Schneider, J. 2010, Pathways Towards Habitable Planets, 430, 409
 Brown, R. A., & Chaffee, F. H., Jr. 1974, ApJ, 187, L125
 Brown, R.A., Goody, R.M., Murcray, F.J., & Chaffee, F.H., Jr. 1975, ApJ, 200, L49
 Brown, R.A. 1976, ApJ, 206, L179
 Brown, R.A., & Shemansky, D. E. 1982, ApJ, 263, 433
 Chiappetti, L. Pierre, M., Adami, C., et al. 2018, A&A, 620, 1
 Christiansen, J.L., Vanderburg, A., Burt, J., et al. 2017, AJ, 154, 122
 Dai, F., Winn, J. N., Arriagada, P., et al. 2015, ApJ, 813, L9
 Dalal S. et al., 2019, arXiv:1906.11013
 Dekker, H., D’Odorico, S., Kaufer, A., Delabre, B., & Kotzłowski, H. 2000, procspie, 4008, 534
 Demory, B.-O., Gillon, M., Madhusudhan, N., & Queloz, D. 2015, MNRAS, 455, 2018
 Dorn, C., Noack, L., & Rozel, A. B. 2018, A&A, 614, A18
 Elkins-Tanton L.T., 2008, E&PSL, 271, 181
 Elkins-Tanton L.T., 2012, AREPS, 40, 113
 Gandolfi, D., Barragán, O., Hatzes, A. P., et al. 2017, AJ, 154, 123
 Golimowski, D.A., Leggett, S.K., Marley, M.S., et al. 2004, AJ, 127, 3516
 Guenther et al. 2011 A&A 525, 24
 Guenther, E.W., Barragán, O., Dai, F., et al. 2017, A&A, 608, A93
 Hu R., Demory B.-O., Seager S., Lewis N., Showman A. P., 2015, ApJ, 802, 51
 Ito, Y., Ikoma, M., Kawahara, H., et al. 2015, ApJ, 801, 144
 Kislyakova, K.G., Fossati, L., Johnstone, C.P., et al. 2018, ApJ, 858, 105
 Kislyakova, K.G., Noack, L., Johnstone, C.P., et al. 2017, Nature Astronomy, 1, 878
 Kupo, I., Mekler, Y., Mekler, Y., & Eviatar, A. 1976, ApJ, 205, L51
 Küppers, M., & Jockers, K. 1995, ApJ, 441, L101
 Küppers, M., & Jockers, K. 1997, Icarus, 129, 48
 Lammer H., et al., 2018, A&ARv, 26, 2
 Léger, A., Rouan, D., Schneider, J., Barge, P., Fridlund, M., Samuel, B., Ollivier, M., Guenther, E., Deleuil, M., Deeg, H. J. et al. 2009, A&A, 506, 287
 Léger A., et al., 2011, Icar, 213, 1
 Miguel, Y., Kaltenegger, L., Fegley, B., et al. 2011, ApJ, 742, L19

- Møller Larsen, J., Modigliani, A., Bramich, D. 2019, UVES Pipeline User Manual, VLT-MAN-ESO-19500-2965
- Morgan, J. S., & Pilcher, C. B. 1982, ApJ, 253, 406
- Mura et al. 2009, Icarus, 200, 1
- Namekata K., et al., 2019, ApJ, 871, 187
- Noack, L., Rivoldini, A., & Van Holst, T. 2016, IJASM, 9, 66
- Noack, L., Rivoldini, A., & Van Holst, T. 2017, Physics of the Earth and Planetary Interiors, 269, 40
- Noll, St., Kausch, W., Barden, M., et al. 2019, VLT-MAN-ESO-19550-5772
- Peale, S. J., Cassen, P., & Reynolds, R. T. 1979, Science, 203, 892
- Rappaport, S., Sanchis-Ojeda, R., Rogers, L. A., Levine, A., & Winn, J. N. 2013, ApJ, 773, L15
- Ridden-Harper, A.R., Snellen, I.A.G., Keller, C. U., et al. 2016, A&A, 593, A129
- Rouan, D., Deeg, H.J., Demangeon, O., et al. 2011, ApJ, 741, L30
- Sanchis-Ojeda, R., Rappaport, S., Winn, J.N., et al. 2013, ApJ, 774, 54
- Schaefer, L., Fegley, B. 2009, ApJ, 703, L113.
- Schleicher et al. A&A, 2004, 425, 1119
- Shalygin, E. V., Markiewicz, W. J., Basilevsky, A. T., et al. 2015, Geophys. Res. Lett., 42, 4762
- Sinukoff, E., Howard, A.W., Petigura, E. A., et al. 2017a, AJ, 153, 70
- Thomas, N. 1993, ApJ, 414, L41
- Thomas, N. 1996, A&A, 313, 306
- Vanderburg, A., Bieryla, A., Duev, D. A., et al. 2016, ApJ, 829, L9
- Vidotto, A., Gregory, S. G., Jardine, M., et al. 2014, MNRAS, 441, 2361
- Winn, J. N., Matthews, J. M., Dawson, R. I., et al. 2011, ApJ, 737, L18
- Winn J. N., Fabrycky D. C., 2015, ARA&A, 53, 409
- Wright, J. T., Marcy, G. W., Butler, R. P., & Vogt, S. S. 2004, ApJS, 152, 261

This paper has been typeset from a $\text{\TeX}/\text{\LaTeX}$ file prepared by the author.